Localization and Imaging of Integrated Circuit Defect Using Simple Optical Feedback Detection

Vernon Julius Cemine*, Bernardino Buenaobra, Carlo Mar Blanca, and Caesar Saloma
National Institute of Physics, University of the Philippines,
Diliman, Quezon City 1101
E-mail: vernon@nip.upd.edu.ph

ABSTRACT

High-contrast microscopy of semiconductor and metal edifices in integrated circuits is demonstrated by combining laser-scanning confocal reflectance microscopy, one-photon optical-beam-induced current (1P-OBIC) imaging, and optical feedback detection via a commercially available semiconductor laser that also serves as the excitation source. The confocal microscope has a compact in-line arrangement with no external photodetector. Confocal and 1P-OBIC images are obtained simultaneously from the same focused beam that is scanned across the sample plane. Image pairs are processed to generate exclusive high-contrast distributions of the semiconductor, metal, and dielectric sites in a GaAs photodiode array sample. The method is then utilized to demonstrate defect localization and imaging in an integrated circuit.

INTRODUCTION

A key concern in semiconductor characterization and device failure analysis is the accurate determination of the electrical current distributions in an integrated circuit (IC) that can divulge the locations of dielectric breakdowns, doping inhomogeneities, electrical overstresses, and inversion layers (Wagner, 2003; Ross & Boit, 1999). Semiconductors, metals, and dielectrics are the main IC material components and characterizing an IC defect requires the accurate identification of the defect material.

Optical beam-induced current (OBIC) imaging is often utilized to determine the two-dimensional (2D) current distribution in an IC sample (Takasu, 2001). Because only semiconductors produce OBIC signals, an exclusive image of the semiconductor sites in an IC sample may be generated by scanning a focused beam

of wavelength $\lambda \leq hc/E_b$, where E_b is the semiconductor band-gap energy, h is Planck's constant, and c is the speed of light in vacuum.

A serious drawback with one-photon (1P) OBIC images is their lack of information concerning the depth distribution of the semiconductor sites in an IC sample. 1P-OBIC images look similar even if taken at different axial positions. Confocal reflectance microscopy yields high-contrast images, but metal and semiconductor sites are difficult to distinguish from each other in these images because both materials exhibit relatively high reflectivities.

It was previously shown that a pair of confocal and 1P-OBIC images could be produced simultaneously from the same focused beam of a modified confocal microscope with an argon-ion laser light source (Daria et al., 2002). We have also developed an image processing procedure for quickly obtaining from the image pair exclusive high-contrast images of the semiconductor, metal, and dielectric sites in an IC sample. The technique was employed to identify

Corresponding author

different kinds of IC defects and their three-dimensional (3D) structures (Miranda & Saloma, 2003).

High-contrast imaging of the semiconductor sites in an IC could also be obtained by two-photon (2P) OBIC (Xu & Denk, 1997; Ramsay et al., 2002). However, the high cost of an ultrafast excitation light source has prevented the 2P-OBIC technique from gaining acceptance as a standard failure analysis tool among IC manufacturers. Acquisition and maintenance costs are primary concerns of the semiconductor industry in selecting a failure analysis tool for their test and assembly lines. The need of industry for more versatile but economical failure analysis tools will grow fast to cope with the increasing architectural sophistication of the next-generation IC devices with very high transistor densities.

Here, we report the localization and imaging of an IC defect with our new inexpensive microscopy technique that obtains high-contrast images of an IC sample (Cemine et al., 2004). Our new technique combines confocal microscopy, 1P-OBIC imaging, and optical feedback (OF) detection with a semiconductor laser (SL). With post-detection processing, the technique permits the generation of exclusive 3D distributions of semiconductors, metals, and dielectric sites.

We have replaced the bulky and inefficient gas laser with the more efficient, smaller, and cheaper SL to excite the IC sample. The SL is also used to detect the optical signals that are reflected from the sample. The microscope features a compact in-line arrangement with no external photodetector (Fig. 1). The OF sensitivity of SLs has been previously utilized in confocal microscopy (Rodrigo et al., 2002) and direction-sensitive velocimetry (Rodrigo et al., 2001).

CONFOCAL REFLECTANCE AND 1P-OBIC IMAGES

We obtain the confocal reflectance image $R(x, y, z)$ by scanning an IC sample relative to a stationary focused SL beam where $R(x, y, z) = |o_r(x, y, z) \otimes h^2(x, y, z)|^2$, $o_r(x, y, z)$ is the true (object) reflection amplitude distribution and $\otimes$ represents a convolution operation. The 1P-OBIC image is given by $C(x, y) = \int o_s(x, y, z) \otimes$

$|h(x, y, z)|^2 dz$, and $o_s(x, y, z)$ is the true distribution of semiconductor materials in the IC sample. The integration is taken from $\pm\infty$. Unlike $R(x, y, z)$, the low-contrast image $C(x, y)$ does contain any information about axial distribution of the semiconductor sites in an IC sample.

The product $S(x, y, z) = R(x, y, z)C(x, y)$ yields an exclusive image of the semiconductor sites at the axial location z (Daria et al., 2002; Miranda & Saloma, 2003). Similarly, $M(x, y, z) = R(x, y, z)C'(x, y)$ yields an exclusive image of the metal sites at the axial plane z, where $C'(x, y) = k - C(x, y)$ and the constant k represents the highest possible $C(x, y)$ pixel value that is measured from the sample.

EXPERIMENT

The experimental setup is shown in Fig. 1. We use a commercially available laser diode (LD) ($l = 833$ nm, Sharp LT015MF) that is operated at 25°C with a LD current/temperature controller (Melles-Grio,t model 06 DLD 105). The power incident on the sample is 22.8 mW. The LD output power is monitored using the built-in photodiode (PD) in the LD package. The divergent and elliptical LD output beam is collimated with a collimating lens (CL) [Melles-Griot, model
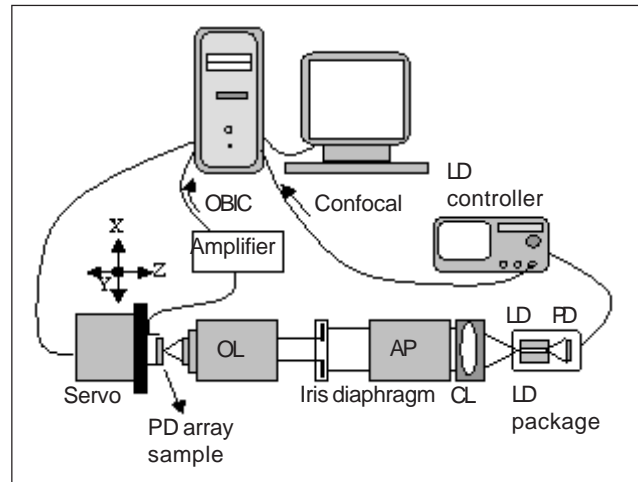
Fig. 1. The combined confocal reflectance and OBIC microscope using a laser diode (LD) source with a built-in photodiode (PD). The collimating lens (CL) has a $f = 14$ mm. The objective lens (OL) has a NA = 0.5 and a $f = 1.7$ mm. Anamorphic prism (AP) is used to partially circularize the beam.

06GLC003, numerical aperture (NA) = 0.276, focal length (f) = 14.5 mm] and circularized by mounted anamorphic prisms (AP) (Melles-Griot, model 06GPA004, 3x magnification). Residual asymmetry in the transverse intensity distribution of the collimated LD beam is removed by the iris diaphragm.

An infinity-corrected objective lens (OL) (Olympus UPlan Fl, nominal NA = 0.5, working distance = 1.7 mm) focuses the LD beam onto the sample that is mounted on a closed-loop *XYZ* servomotor stage (Thorlabs, model PT3-Z6) which is driven by a motion-controller card (Thorlabs, DCX-PCI100). All stage-scanning and image acquisition protocols are coded using LabVIEW 7.0 (National Instruments). Analog-to-digital conversion of the PD and 1P-OBIC signals is accomplished with a 12-bit data-acquisition board (National Instruments, model 6024E; conversion rate: 200 kHz).

RESULTS AND DISCUSSION

The axial responses for the confocal reflectance and OBIC microscopes are obtained at a particular site in the photodiode array sample. The responses are shown in Fig. 2.

Confocal reflectance signal varies with axial position, while the OBIC signal is approximately constant as exhibited in Fig. 2. This manifests the axial sectioning
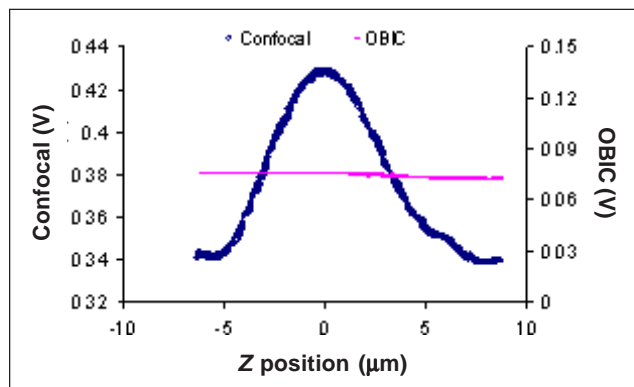
Fig. 2. Axial responses for confocal reflectance and OBIC microscopes. Axial sectioning is observed by the confocal reflectance microscope. The OBIC microscope, on the other hand, exhibits no dependence with the axial position. Effective NA for the OL here is 0.39.

capability of the confocal reflectance microscope and the limitation of the OBIC microscope for depth discrimination. The axial sectioning capability of the confocal reflectance microscope is brought about by the rejection of the out-of-focus beams that are reflected back by the sample to the LD front facet, which serves as the confocal pinhole. On the other hand, the inability of the OBIC microscope to attain axial sectioning is caused by the fact that the OBIC signal is the sum of all the currents generated at all axial positions that are being irradiated with light of photon energy higher than the band gap of a semiconductor *p-n* junction. This total of the generated currents does not vary significantly as the focus of the beam is scanned along the different axial positions.

Despite the limitation of OBIC imaging to axial sectioning, this imaging technique is capable of discriminating semiconductor parts from metal parts (and vice versa) in an observation site.

We can endow axial discrimination to OBIC imaging and thereby build up a 3D representation of exclusive semiconductor and metal sites by the numerical process enumerated in the methodology. The result is shown in Fig. 3, where the 200 mm x 200 mm confocal, OBIC, semiconductor, and metal images of a particular site in a PD array sample at different axial positions, $Z = -4$, 0, and, 4 mm, are exhibited. The semiconductor images are obtained from the multiplication of the confocal and OBIC images. Metal images are obtained from the multiplication of the OBIC complement and the confocal images.

Axial sectioning is clearly exhibited by the high-contrast confocal images. Notice the differing intensity and the parts that are being highlighted as the axial position changes. Axial sectioning is not exhibited by the low-contrast OBIC images, but notice the discrimination between the semiconductor part (high intensity) and metallic part (low intensity). The semiconductor part is the one that produces a high OBIC signal when irradiated and is thus the high-intensity portion of the OBIC image. The metal part, on the other hand, produces a low OBIC signal when irradiated and is thus the low-intensity part of the image. Upon multiplying the confocal and OBIC images, high-contrast images of the semiconductor sites (highlighted part)
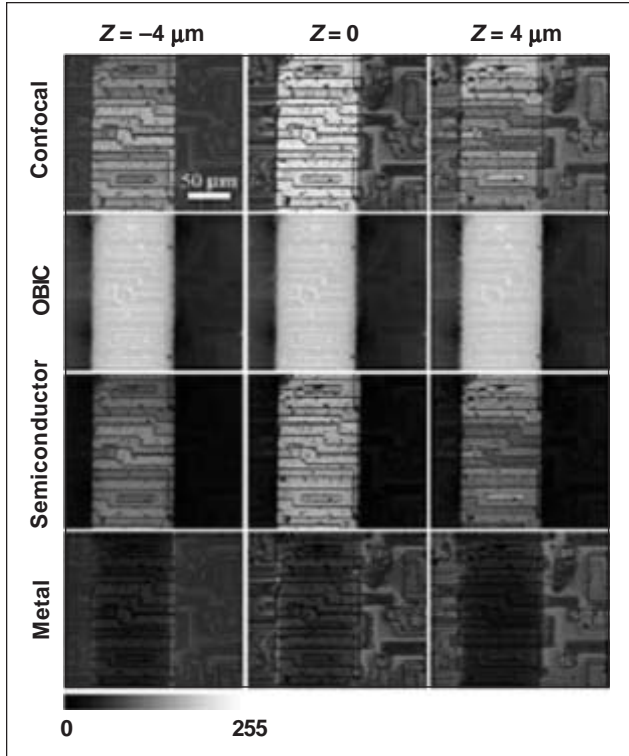
Fig. 3. 200 mm x 200 mm confocal, OBIC, semiconductor, and metal images of a portion of the PD array sample at different axial positions. Axial sectioning is observed by the high-contrast confocal images. Semiconductor and metal discrimination is observed by the low-contrast OBIC images. High-contrast semiconductor images are obtained from confocal and OBIC multiplication. High-contrast metal images are obtained from OBIC complement and confocal image multiplication. Effective NA for the OL here is 0.39.

are obtained. Moreover, axial sectioning is observed on the resulting images as exhibited by the differing semiconductor intensity as the axial position changes. High-contrast images of the metal portions on the observation site are observed upon multiplying the OBIC complement and confocal images. Just like the semiconductor sites, axial sectioning is also observed on the resulting images as exhibited by the differing metal intensity and intensity distribution as the axial position changes.

A particular strength of this protocol is the ease with which the metal and semiconductor parts are mapped out, making it effective in exactly situating defective sites.

Figure 4 shows the 200 mm x 200 mm (a) confocal, (b) OBIC, (c) metal, and (d) semiconductor images of a site in an IC (Z84C0008FEC) with a verified electrical
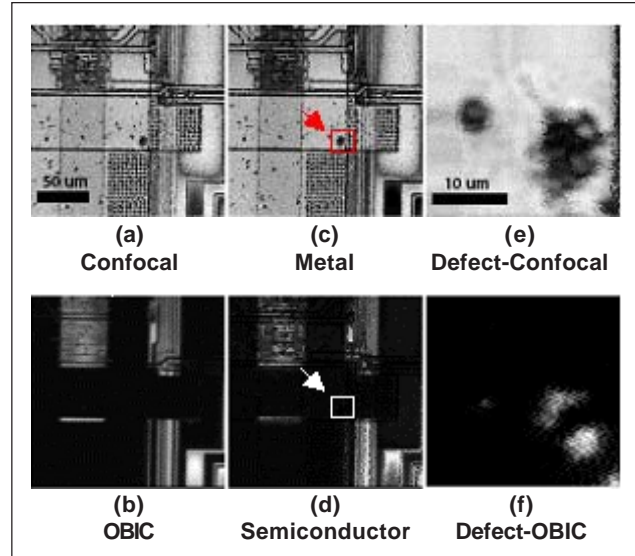
Fig. 4. 200 mm x 200 mm (a) confocal, (b) OBIC, (c) metal, and (d) semiconductor images of a portion of an IC (Z84C0008FEC) with EOS (boxed part). 25 mm x 25 mm or zoomed (e) confocal and (f) OBIC images of the EOS.

overstress (EOS) defect (boxed). Imaging is done at the focus ($Z = 0$) using a 780 nm LD (Sharp LT024MD). The third column is a magnified shot (25 mm x 25 mm) of the (e) confocal and (f) OBIC images of the EOS defect, that is, the portion pointed by the arrows on the second column.

It is apparent in Figs. 4(c) and 4(d) that the EOS is situated on the metallic portion of the IC. Zooming in on the EOS site, however, reveals a small OBIC signal generation [see Fig. 4(f)], a possible leakage or current bleedthrough across the metal and the underlying semiconductor layers. The leakage current ranges from 60–150 nA, which is amplified using a current preamplifier (GW specimen current amplifier type 103B/31). Investigation on the exact nature of the phenomenon is still currently being undertaken. Nevertheless, it was shown here that an IC defect can be localized and discriminated from the normal portions through its abnormal OBIC signal generation.

CONCLUSION

We have demonstrated an inexpensive technique for high-contrast imaging of semiconductor and metal sites in an IC sample. The OF microscope which utilizes an

SL for both sample excitation and detection is compact and economical. SLs are versatile light sources that can be acquired cheaply at various emission wavelengths. The SL output wavelength is easily tuned by varying the cavity temperature or injection current. High-contrast imaging is demonstrated by distinguishing the three-dimensional distributions of semiconductor, metal, and oxide sites in a photodiode array sample.

Despite the low incident power on the sample, the method was sensitive enough to detect current in the 60–150 nA range leaking through an EOS defect site. The simple and compact optical setup makes for a cost-effective failure analysis tool that can open the road to affordable, table-top semiconductor characterization and defect analysis.

REFERENCES

Cemine, V.J., B. Buenaobra, C.M. Blanca, & C. Saloma, 2004. High-contrast microscopy of semiconductor and metal sites in integrated circuits via optical feedback detection. *Opt. Lett.,* 2004 **29**: 2479-2481.

Daria, V., J. Miranda, & C. Saloma, 2002. High-contrast images of semiconductor sites via one-photon beam-induced current imaging and confocal reflectance microscopy. *Appl. Opt*. **41**: 4157–4161.

Miranda, J. & C. Saloma, 2003. Four-dimensional microscopy of defects in integrated circuits. *Appl. Opt*. 42: 6520–6524.

Ramsay, E., D. Reid, & K. Wilsher, 2002. Three-dimensional imaging of a silicon flip chip using the two-photon optical beam-induced current effect. *Appl. Phys. Lett.* **81**: 7–9.

Rodrigo, P., M. Lim, & C. Saloma, 2002. Direction-sensitive subwavelength displacement measurements at diffraction-limited resolution. *Opt. Lett*. **27**: 25–27.

Rodrigo, P., M. Lim, & C. Saloma, 2001. Optical-feedback semiconductor laser Michelson interferometer for displacement measurements with directional discrimination. *Appl. Opt.* **40**: 506–513.

Ross, R. & C. Boit (eds.), 1999. Microelectronic failure analysis desk reference, 4th ed. ASM International, Materials Park, OH.

Takasu, S., 2001. Application of OBIC/OBIRCH/OBHIC: Semiconductor failure analysis. *JEOL News*. **36E**: 60–63.

Wagner, L., 2003. Trends in failure analysis. *Microelectron. Reliab.* **43**: 1369–1375.

Xu, C. & W. Denk, 1997. Comparison of one- and two-photon optical beam-induced current imaging. *J. Appl. Phys.* **86**: 2226–2231.